Chemical Science

RSC Publishing

EDGE ARTICLE

View Article Online
View Journal | View Issue

Cite this: *Chem. Sci.*, 2013, **4**, 3432

Floating conductive catalytic nano-rafts at soft interfaces for hydrogen evolution†

Xiaojun Bian,[ab] Micheál D. Scanlon,[b] Sinong Wang,[a] Lei Liao,[a] Yi Tang,[a] Baohong Liu[a] and Hubert H. Girault*[b]

Received 9th May 2013
Accepted 5th July 2013

DOI: 10.1039/c3sc51290h

www.rsc.org/chemicalscience

Mo_2C nanowires and composites of Mo_2C nanoparticles formed on multiwalled carbon nanotubes (Mo_2C/CNT) were developed as advanced catalysts for hydrogen evolution at a polarised water–1,2-dichloroethane interface. Each catalyst acts as a catalytic nano-raft suspended at the interface to markedly enhance the rates of biphasic proton reduction in the presence of an organic solubilised electron donor, decamethylferrocene. Mo_2C nanoparticles were grown *in situ* on the conductive CNT support, achieving a high dispersion and intimate contact, thereby facilitating electron transfer between the components. The high catalytic activity of each catalyst was successfully demonstrated by their respective impacts on the reaction kinetics. The reaction rate increased more than 1000 times when the Mo_2C/CNT composite was present at a very low concentration of 25 μM. CNTs have the ability to act as highly efficient conduits or "transport superhighways" for injected electrons to reach the catalytic sites of the nanoparticle. Electrochemical instabilities, similar to those observed for the transfer of surface-active ions, were observed under experimental conditions that produced an abundance of hydrogen at the interface. Finally, the movement of CNTs floating at the interface under the influence of a cycling applied interfacial Galvani potential difference was vividly captured in a short movie.

Introduction

The development of novel methodologies and active catalysts based on earth-abundant materials to achieve the Hydrogen Evolution Reaction (HER), whereby aqueous protons are reduced to molecular hydrogen (H_2), is of vital technological importance for future solar-based carbon-neutral energy production.[1] A methodology, and an accompanying theory, has been developed to reduce protons at defect free electrified oil–water interfaces.[2] Protons may be pumped from the aqueous to the oil phase (1,2-dichloroethane (1,2-DCE)) by careful control of the interfacial Galvani potential difference ($\Delta_o^w\phi$), either potentiostatically or chemically (by distribution of electrolyte ions), and subsequently reduced to H_2 using organic reducing agents, thus far typically metallocenes.[2b,3]

This biphasic HER may be catalysed by floating interfacial H_2 evolution catalysts (HECs), as demonstrated for both well known (molybdenum sulphide, MoS_2)[4] and recently reported (molybdenum carbide (Mo_2C) and boride (MoB))[5] non-precious metal-based HECs. However, the reaction kinetics for H_2 production are still limited in these systems and, thus, it is crucial to design new catalysts with higher activities. The biphasic HER, while less-well documented, is subject to the same trends in catalysis as observed for single phase HERs, *i.e.* immobilising MoS_2 on reduced graphene oxide (RGO) or mesoporous carbon increases the rates of reaction in comparison to "free" MoS_2 as dramatically for a biphasic reaction, with decamethylferrocene (DMFc) injecting electrons into the carbon support,[6] as for a single phase reaction.[7]

Carbon allotropes (primarily carbon nanotubes (CNTs),[8] graphene,[9] and fullerenes[10] but also carbon nanodots,[11] mesoporous carbon nanospheres[12] or graphene foams,[13] *etc.*) provide conductive scaffolds for next-generation composite materials. Single or multicomponent[14] systems may be rationally designed on a single support incorporating one, or a combination, of catalytic metallic (*e.g.* Pt,[15] Au,[16] or Pd (ref. 17)), non-precious (*e.g.* MoS_2 (ref. 13*a* and 18)) or semiconducting (*e.g.* TiO_2 (ref. 14*c* and 19)) nanoparticles (NPs). Individual carbon composites may be tailored to achieve a myriad of functions including the provision of an integrated platform to store and convert solar energy,[20] single-substrate multi-step heterogeneous catalysis (*e.g.* towards the HER),[21] or sensing applications.[22] Carbonaceous materials are typically insoluble particulates both in aqueous and oil phases and, driven by the requirement to

[a]*Department of Chemistry and Laboratory of Molecular Catalysis and Innovative Materials, Centre of Chemistry for Energy Materials, Fudan University, Shanghai 200433, P. R. China*

[b]*Laboratoire d'Electrochimie Physique et Analytique, École Polytechnique Fédérale de Lausanne (EPFL), Station 6, CH-1015 Lausanne, Switzerland. E-mail: Hubert.Girault@epfl.ch; Fax: +41 21 6933667*

† Electronic supplementary information (ESI) available: Experimental procedures and a movie of carbon nanotubes moving at the liquid–liquid interface under the influence of an applied interfacial Galvani potential difference. See DOI: 10.1039/c3sc51290h

minimise the interfacial free energy in the system, will self-assemble and float at the liquid–liquid interface.[23] Thus, the liquid–liquid interface represents a novel, experimentally reproducible and thus far underdeveloped, platform at which to exploit the use of these floating rafts with a veritable Swiss Army Knife range of functionality.

A series of synergistic catalytic benefits are accrued by incorporating a carbon support in catalyst design.[21a] Growing a catalyst, such as MoS_2,[7,12,13,18] directly on a carbon scaffold leads to (a) a significant decrease in the average NP size in comparison to an identical synthesis in the absence of a scaffold (*i.e.* in effect vastly increasing the quantity of exposed surface catalytic sites), (b) a highly dispersed distribution of catalyst NPs on the high specific area support, again maximizing the availability of exposed surface catalytic sites, and (c), for catalysts immobilized on an electrode's surface[12,13,18] or present as aqueous dispersions,[7] the provision of a low resistance "transport superhighway" for injected electrons to travel from the electrode,[12,13,18] a strong molecular electron donor,[6] the semi-conductor conduction band[14c,19] or an excited dye[7] to the catalyst's active site. The latter benefit enables charge carrier collection or a "pool of electrons" to accumulate on the carbon support, thereby increasing the cross-section of reaction of the catalyst composite with the electron donating element. The dominant synergistic effect is the quality of the interfacial electrical contact between the carbon support and the catalyst, as demonstrated by a recent systematic comparison by Kim and Park of the relationship between photocatalytic H_2 evolution activity and the bulk physicochemical properties of several carbon supports using carbon/CdSe composites as a model system.[24]

Taking into account the catalytic benefits associated with nano-sizing a catalyst and the synergistic benefits obtainable by growing a catalyst on a carbon support, in this article we have designed advanced catalysts to improve the reaction activity in a biphasic HER system. We compare the activities of three successively more advanced generations of the catalyst Mo_2C towards the biphasic HER. Generation 1 is simply micron-sized commercial Mo_2C and represents the least optimal, baseline activity exhibited by this catalyst. Generation 2 is a porous Mo_2C nanowire, expected to exhibit the catalytic benefits associated with nano-sizing a catalyst (more exposed active sites *etc.*) and containing an enriched porosity (possible nano-confinement effects and further increases in the catalytic surface area). Finally, generation 3 involves the growth of Mo_2C NPs on a CNT support (CNT/Mo_2C), with all the benefits expected as described *vide supra*. This study clearly highlights the dominance of the electrical contact between the carbon support and the catalyst over the benefits obtained by simply nano-sizing the catalyst. Insights are gained into the injection of electrons from an organic solubilised electron donor (DMFc) to a carbon support (CNTs, specifically multiwalled carbon nanotubes (MWNT)) floating at a liquid–liquid interface, and the subsequent use of these electrons *via* a Mo_2C catalyst supported on CNTs to reduce organic solubilised or interfacial protons under the influence of an applied interfacial Galvani potential difference. The appearance of electrochemical instabilities in specific potential regions when high rates of H_2 evolution occur is discussed and the movement of these floating carbon rafts at the interface upon cycling the applied interfacial potential is scrutinized.

Results and discussion

Catalyst characterisation

Nanowire Mo_2C and CNT/Mo_2C were both synthesised from a common inorganic–organic Mo_3O_x/amine hybrid composite precursor *via* pyrolysis[25] or an impregnation process,[26] respectively (precursor characterisation was reported by one of us previously).[25] In both procedures the intercalating amine has a dual synthetic function as a reducing agent and carbide carbon source (experimental details of each synthesis in ESI†).[25,26] Mo_2C nanowires possess uniform 1-D morphologies, being several microns in length and 80–150 nm in width (see scanning electron microscopy (SEM) and transmission electron microscopy (TEM) images, Fig. 1A and C). However, when scrutinized by high-resolution TEM (HR-TEM, Fig. 1E) the individual nanowires were revealed to consist of discrete Mo_2C nanocrystals, *ca.* 10 to 15 nm in size. The X-ray diffraction (XRD) pattern was consistent with the presence of the pure hexagonal β-Mo_2C phase (JCPDS: 35-0787, Fig. 1F and S1, ESI†). TEM images of CNT/Mo_2C reveal the highly dispersed nature of the individual *ca.* 10 nm Mo_2C NPs on the CNT surface (Fig. 1B). The individual Mo_2C NPs may be clearly observed by HR-TEM (Fig. 1D). The XRD pattern of CNT/Mo_2C was consistent with the presence of the pure hexagonal β-Mo_2C phase (JCPDS: 35-0787)

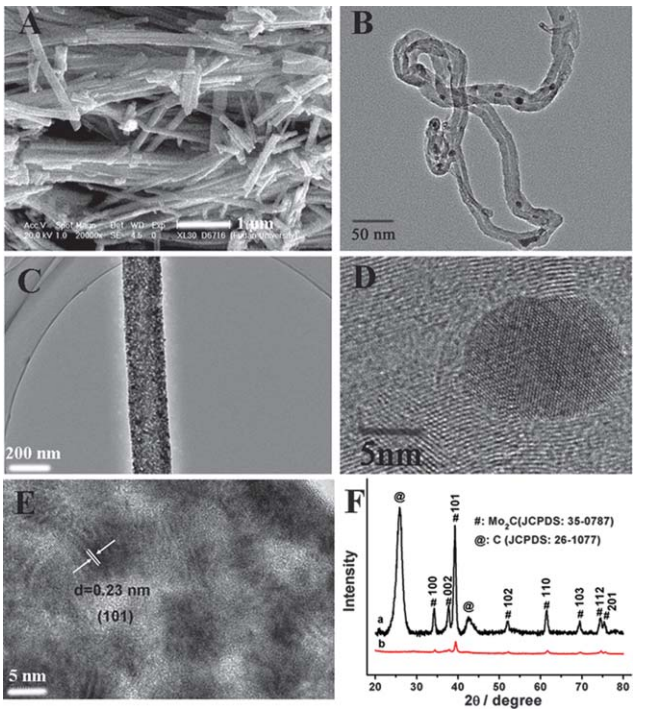

Fig. 1 Scanning electron microscopy (SEM) image of (A) nanowire Mo_2C; transmission electron microscopy (TEM) images of (B) Mo_2C/CNT and (C) nanowire Mo_2C; high resolution-TEM (HR-TEM) images of (D) CNT/Mo_2C and (E) nanowire Mo_2C; (F) X-ray diffraction (XRD) patterns of (a) Mo_2C/CNT and (b) nanowire Mo_2C. The XRD of nanowire Mo_2C is expanded to full size in Fig. S1, ESI.†

and carbon attributable to the CNT support (JCPDS: 26-1077, Fig. 1F). The BET surface areas of nanowire Mo_2C and CNT/Mo_2C were *ca.* 54 and 150 $m^2\ g^{-1}$, respectively, as previously reported.[25,26] An in-depth characterisation of the commercial Mo_2C samples used in this study has been presented previously.[5,27] Briefly, commercial Mo_2C with particle sizes in the range 1–3 μm was found by XRD to be exclusively in the pure hexagonal β-Mo_2C phase (space group $P6_3/mmc$) and possess negative ζ-potentials under basic and acidic conditions (pH range studied: 2 to 10) due to the presence of some surface oxides, *e.g.* MoO_4^{2-}.

Quantitative evaluation of biphasically evolved H_2 for each floating Mo_2C-based catalyst

The relative catalytic activities of commercial (micron-sized) Mo_2C, nanowire Mo_2C and CNT/Mo_2C towards biphasic HER were initially investigated by monitoring the quantities of H_2 evolved after 1 hour from shake flask experiments by gas chromatography (see Scheme 1; experimental details in ESI†) and compared with a shake flask with only unfunctionalised CNTs present or devoid of catalyst under anaerobic conditions (Fig. 2). On contacting the acidic aqueous (w) and 1,2-DCE (o) phases, an interfacial Galvani potential difference ($\Delta_o^w\phi$) was established due to the distribution of lipophilic tetrakis-(pentafluorophenyl)borate anions (TB^-). Consequently, with TB^- acting as a phase transfer catalyst, protons were extracted or "pumped" to 1,2-DCE almost quantitatively (see previous calculations[5] for commercial Mo_2C at the equilibrium concentrations (mM) of each of the constituent ions for the shake flask outlined in Scheme 1) as hydrogen tetrakis(pentafluorophenyl)-borate diethyletherate (HDEETB, referred to hereafter as HTB for simplicity). Diethyletherate (DEE) acts as a lipophilic base. The chosen organic electron donor, DMFc, is insoluble in the aqueous phase and electron injection can be considered to take place exclusively in 1,2-DCE. The majority of the insoluble Mo_2C-based catalysts float at the interface, preferentially adsorbing to minimise the interfacial free energy in the system. Thermodynamically, only organic solubilized protons with a redox potential *versus* the standard hydrogen electrode in 1,2-DCE $\left(\left[E^0_{H^+/\frac{1}{2}H_2}\right]^{1,2\text{-DCE}}_{SHE} = 0.55\ V\right)$ (ref. 2*b*) or interfacial aqueous protons under the influence of an applied $\Delta_o^w\phi > 0.55$ V have sufficiently positive redox potentials to be reduced by DMFc $\left(\left[E^0_{DMFc^{0/+}}\right]^{1,2\text{-DCE}}_{SHE} = 0.04\ V\right)$.[28] The evolution of H_2 proceeds until the supply of DMFc or HTB (depending on which is in excess) is exhausted, the global reaction being:

$$DMFc^o + H^{+,w} \xrightarrow{\text{catalyst}} DMFc^{+,o} + \frac{1}{2}H_2 \qquad (1)$$

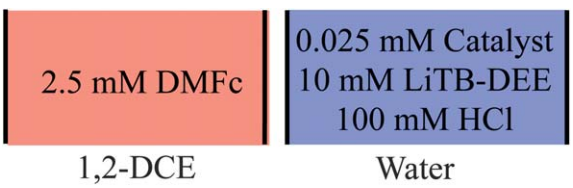

Scheme 1 Chemical polarisation of the interface: schematic representation of the initial compositions of the aqueous and organic phases, with the catalyst suspended at the interface, used to perform the biphasic H_2 evolution reaction *via* shake flasks. The products of the biphasic reactions, H_2 and $DMFc^+$ (see eqn (1)), were monitored by gas chromatography and UV/vis spectroscopy, respectively.

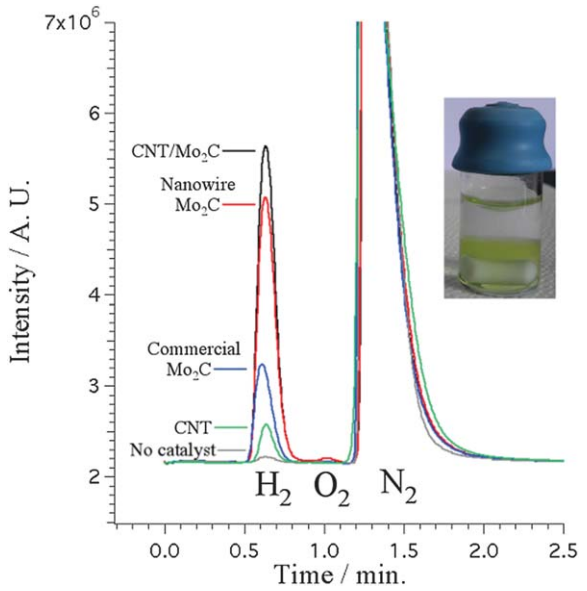

Fig. 2 Gas chromatograms of the shake flask headspace for biphasic H_2 evolution reactions (see Scheme 1) after 1 h, under anaerobic conditions, both in the absence and presence of each floating catalytic nano-raft, as indicated. Inset: GC shake flask glass vial.

The kinetically slow non-catalysed biphasic HER evolved 0.052 μmol H_2 after 1 h, representing just 2.08% of the maximum theoretical stoichiometric amount of H_2 (2.5 μmol), as limited by the initial [DMFc] in 1,2-DCE (5 μmol) and the very small quantity of H_2 dissolved in the liquid phases. The rates of reaction increased dramatically in the presence of the floating catalyst with 0.606, 1.676, and 1.99 μmol H_2 detected for commercial Mo_2C, nanowire Mo_2C and CNT/Mo_2C, respectively, after 1 h. The control experiment with unfunctionalised CNTs also exhibited an increased production of H_2 (0.125 μmol) relative to the baseline response. This indicates that even though the CNTs used were >90% pure, some remaining trace metallic impurities do give the CNTs a small intrinsic H_2 evolving ability of their own. This is in contrast to a mesoporous carbon substrate, which exhibits no H_2 evolution activity due to its ease of preparation in the absence of metal.[6] As shown in Fig. 2 (and by spectroscopic and voltammetric measurements, *vide infra*), however, the catalysis by trace impurities in the CNT is minor compared with that exhibited by the Mo_2C/CNT nanocomposite.

Enhanced biphasic HER reaction kinetics for each generation of floating Mo_2C-based catalysts

The influence of each Mo_2C-based catalyst on the rate of H_2 evolution may be probed by monitoring changes in the

concentration of the other reaction product, the organic solubilised decamethylferrocenium cation, $DMFc^+$, (see eqn (1)), with time by UV/vis spectroscopy (see Scheme 1 and Fig. 3; experimental details in ESI†). Identical rate orders with respect to DMFc and protons were obtained for nanowire Mo_2C and CNT/Mo_2C, respectively, as described previously (data not shown).[5] The rate constants were calculated by fitting (see Fig. 4A and Table 1),[5] and used to determine the theoretical $[DMFc^+]$ in 1,2-DCE as a function of time in the presence of each catalyst. The experimental results were reproduced (plotted using a logarithmic scale for clarity for the reaction time in Fig. 4B) confirming the validity of the assumed rate equations. Due to the extremely slow rates of reaction both in the absence of catalyst and presence of unfunctionalised CNTs, the polynomial fits were inadequate to confidently stipulate specific reaction orders and, thus, this data was not fitted. Enhanced kinetics in the presence of the floating CNT/Mo_2C catalyst permitted the maximum stoichiometric amount of $DMFc^+$ (2.5 mM), limited by the initial [DMFc] (2.5 mM), to be attained after 600 s (Table 1), epitomizing the vastly superior conversion rate of protons to H_2 compared to that in the absence of catalyst (*ca.* 1%) or presence of only CNTs (*ca.* 6%) and a significant outperformance of commercial Mo_2C (8%) and even nanowire Mo_2C (65%). Indeed, if an assumption of first order kinetics is assumed for all shake-flask reactions, CNT/Mo_2C improves the rates of catalysis more than 1000-fold when compared to a non-catalysed reaction and 600-fold compared to the minor catalysis observed due to trace metallic impurities in the CNT substrate.

The catalytic efficiency of nanowire Mo_2C towards the biphasic HER is significantly enhanced compared to micron-sized commercial Mo_2C due to a favourable combination of nanoscale catalyst dimensions, the rich porosity of each individual nanowire and the presence of large surface areas free from inactive deposits of carbon (confirmed previously by Raman spectroscopy).[25] Such a combination of attributes provides abundant specific catalytic sites for reaction while also facilitating the access of electrolytes and allowing fast charge transfer kinetics. CNT/Mo_2C, while also profiting catalytically from an abundance of specific catalytic sites due to the large dispersion of Mo_2C NPs impregnated on the high specific surface area CNT support, crucially also benefits from the provision of alternative conductive pathways to each Mo_2C NP active site. This key attribute of carbon scaffolds, their large capacities to accept, store and, under the correct circumstances, discharge multiple electrons,[29] definitively improves the observed catalysis. Additionally, very recently, Adzic and co-workers[30] reported that the covalent binding between Mo_2C and the CNT support induces a charge transfer from molybdenum

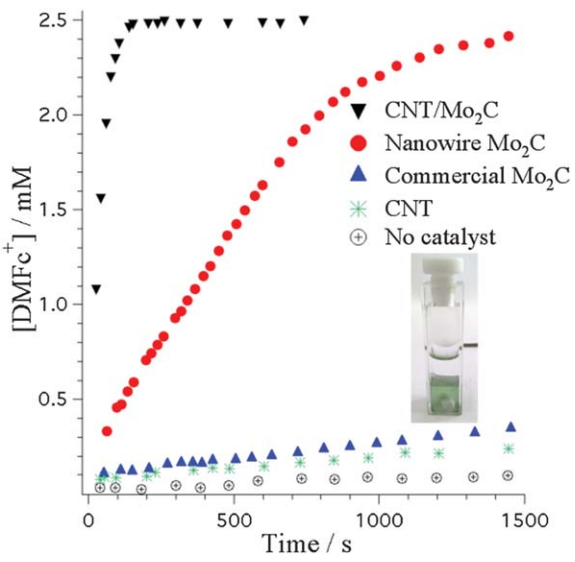

Fig. 3 Kinetics of the biphasic H_2 evolution reaction (HER) with chemically controlled polarization (see Scheme 1) in the absence and presence of each floating catalytic nano-raft, as followed by monitoring changes in the UV/vis absorbance (λ_{max} = 779 nm) for organic solubilized $DMFc^+$. Inset: kinetics UV/vis quartz cuvette.

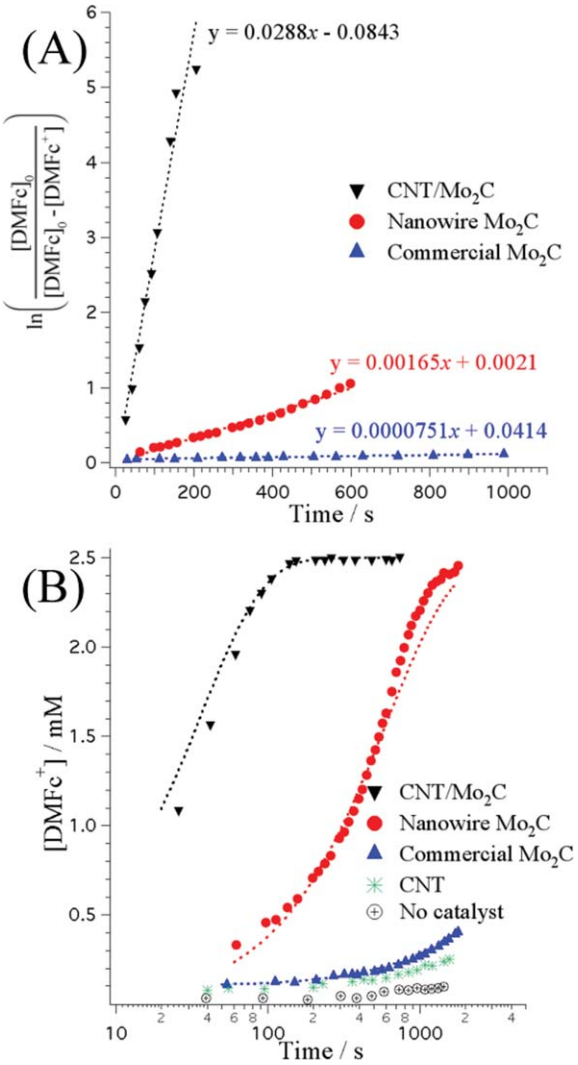

Fig. 4 (A) Determination of the rate constants (k): plots of the integrated rate law *versus* time (s) for the biphasic H_2 evolution reactions of commercial Mo_2C, nanowire Mo_2C and CNT/Mo_2C, each exhibiting 1st order kinetics. $[DMFc]_0$ is the initial concentration of DMFc at $t = 0$ s. The slopes of the straight lines represent the rate constants (k/s^{-1}) for a 1st order reaction for each catalyst, tabulated in Table 1. The composition of the biphasic cell is outlined in Scheme 1. (B) The initial rates of reaction are clarified by using a logarithmic scale for the reaction time. Fits (dotted lines) were obtained from the calculated rate constants (k/s^{-1}).

Table 1 The conversion rate of $[DMFc]_0$ (initial concentration of DMFc at $t = 0$ s) to $[DMFc^+]$ after 600 s (%) and the calculated apparent rate constants (k/s^{-1}) for the biphasic HER in the presence and absence of each catalyst, see Scheme 1

Catalyst	Conversion rate/%	k/s^{-1}
CNT/Mo_2C	100	0.0288
Nanowire Mo_2C	65	0.00165
Commercial Mo_2C	8	0.000075
CNT	6	0.000048[a]
No catalyst	1	0.000023[a]

[a] These values are based on an assumption that 1st order kinetics are obtained in the absence of catalyst or presence of CNTs only and presented simply for comparison. Due to the extremely slow rate of reaction in the absence of catalyst and the presence of CNTs, the polynomial fits were inadequate to confidently stipulate a specific reaction order.

to carbon, downshifting the d-band center of molybdenum. This, in effect, decreases its hydrogen binding energy and eases the electrochemical desorption of an adsorbed hydrogen atom. The resultant relatively moderate Mo–H binding strength for Mo_2C/CNT may contribute to the enhanced HER.

Probing the mechanism of catalysis for floating catalytic rafts *via* voltammetry at the liquid–liquid interface

The potential window of a cyclic voltammogram (CV) obtained at a potentiostatically polarised liquid–liquid interface is typically limited by the ion transfer of the background electrolytes. Herein, the baseline response at *ca.* pH 3 (see Scheme 2, $x = 0$, $y = 0$, $z = 0.5$, and Fig. 5; experimental details in ESI†) was limited by reversible proton and SO_4^{2-} transfer, with some undissociated HSO_4^- transferring also, at the positive and negative potential limits, respectively. In the presence of the organic electron donor DMFc (see Scheme 2, $x = 2.5$, $y = 0$, $z = 0.5$, and Fig. 5) a small current wave at positive potentials was observed and the reverse peak remains due to incomplete consumption of protons, as reported previously.[6] Meanwhile, a reversible transfer peak at $\Delta_o^w\phi = -0.26$ V is indicative of the biphasic reaction product $DMFc^+$ (or, perhaps, the intermediate DMFc-hydride species) undergoing ion transfer.[6]

A series of control experiments clearly indicated that in the presence of *both* a floating interfacial catalyst and the organic electron donor increased rates of proton consumption (and, thus, H_2 evolution) were evident (see Scheme 2, $x = 2.5$, $y = 0.1$, $z = 0.5$, and Fig. 5). Firstly, irreversible current waves at positive potentials were observed and attributed to a proton coupled electron transfer (PCET) event whereby interfacial or organic transferred protons adsorbed on the catalyst's surface undergo rapid electron transfer with either DMFc, for commercial Mo_2C

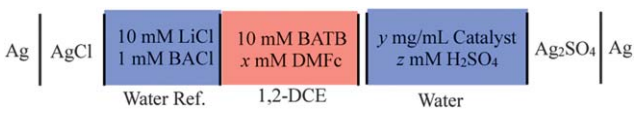

Scheme 2 Potentiostatic polarisation of the interface: schematic representation of the composition of the electrochemical cells used for ion transfer voltammetry.

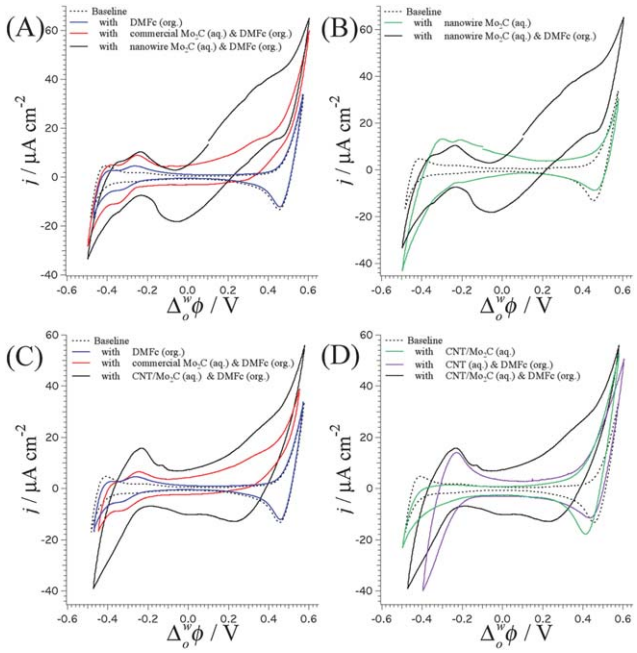

Fig. 5 The catalytic proton coupled electron transfer (PCET) responses for (A and B) nanowire Mo_2C and (C and D) CNT/Mo_2C (black lines, $x = 2.5$, $y = 0.1$, $z = 0.5$) are compared with those for the baseline response (dashed lines, $x = 0$, $y = 0$, $z = 0.5$), in the presence of DMFc only (blue lines, $x = 2.5$, $y = 0$, $z = 0.5$), in the presence of commercial Mo_2C (red lines, $x = 2.5$, $y = 0.1$, $z = 0.5$), in the presence of either catalyst but absence of DMFc (green lines, $x = 0$, $y = 0.1$, $z = 0.5$), and, for specific comparisons with CNT/Mo_2C, in the presence of CNT (purple line, $x = 2.5$, $y = 0.1$, $z = 0.5$). All electrochemical cells were set up as described in Scheme 2. Scan rate: 50 mV s^{-1}.

and nanowire Mo_2C, or both DMFc and electrons "pooled" in the carbon support for CNT/Mo_2C. Secondly, the absence of a return peak for proton transfer from 1,2-DCE to the aqueous phase was noted and attributed to the heterogeneous evolution of H_2 fully consuming the protons, according to eqn (1). Thirdly, the $DMFc^+$ transfer current wave increased in magnitude in the negative potential region in comparison to the situation without a catalyst present, again according to eqn (1). Finally, a visibly rapid increase in the rate at which H_2 bubbles nucleate and grow at the interface after successive CVs was evident. Taking each of these observations into account we may conclude that the voltammetry starkly highlights the improvements in catalysis shown by both nanowire Mo_2C (Fig. 5A) and CNT/Mo_2C (Fig. 5C) *versus* commercial Mo_2C. Additionally, none of these tell-tale catalytic CV features appeared in the absence of DMFc, even with the catalyst floating at the interface (see Scheme 2, $x = 0$, $y = 0.1$, $z = 0.5$, and Fig. 5B and D).

The largest $DMFc^+$ transfer peak was observed for the electrochemical cell with CNT/Mo_2C floating at the interface and DMFc present in the organic phase (Fig. 5D). Initially, since CNT/Mo_2C was clearly shown to be the most active catalyst by the shake flask reactions, an assumption was made that this large $DMFc^+$ transfer peak was simply due to the faster PCET reaction in the presence of this catalyst and a subsequent associated enhanced production of $DMFc^+$, as per eqn (1), within the time-frame of the CV. However, a control experiment

with floating unfunctionalised CNTs at the interface in the presence of DMFc in 1,2-DCE exhibited a marked increase in the magnitude of the $DMFc^+$ transfer current peak in comparison to that in the absence of catalyst (or, indeed, in the presence of highly active nanowire Mo_2C) but matched that observed for CNT/Mo_2C (Fig. 5D). Thus, the increase in conversion of DMFc to $DMFc^+$ indicates that CNTs act as a reservoir of electrons at the interface. As shown *vide supra*, control shake flask experiments with CNTs at the interface (as in Scheme 1) showed some signs of catalysis towards the biphasic HER due to trace metal impurities. However, the smaller magnitude of H_2 evolved (Fig. 2), the slower kinetics for $DMFc^+$ formation exhibited (Fig. 3 and Table 1) and the absence of an obvious PCET transfer wave in the positive potential region of the CV (Fig. 5D) for CNTs *versus* CNT/Mo_2C all indicate that the majority of the "pooled" electrons in the CNT support remain unused at the interface in the absence of a catalyst.

In essence, while the reported work functions of MWNTs, Φ_{MWNT}, suggest that thermodynamically the carbon support may be capable of using stored electrons to reduce organic solubilised or interfacial protons under the influence of an applied positive $\Delta_o^w\phi$ (discussed below), in reality the Mo_2C catalyst is required to act as a "gate" through which these "pooled" electrons may kinetically flow to reduce the adsorbed protons at active sites *via* a PCET process. The use of carbon supports as electron reservoirs is well documented. Fullerene (C_{60}), exhibiting multiple stepwise reductions, has been described as an "electron sponge".[10,31] Meanwhile, Kamat and co-workers have elegantly shown that both RGO[14c,32] and CNTs[19a,33] act as highly effective reservoirs of electrons (in the case of single walled nanotubes (SWNTs) storing up to one electron per 32 carbon atoms[19a]). A carbon allotrope may accept electrons from a donor species with a more reducing redox potential than it's own work function. The potentials quoted in this discussion on the standard hydrogen electrode (SHE) scale are related to the absolute vacuum scale (AVS) by −4.44 eV.[34] Photoexcited molecular species such as methyl viologen radicals, $\left[E^0_{MV^{2+}/MV^{+\bullet}}\right]_{SHE} = -0.45$ V,[35] the conduction band of photoexcited semiconductors such as TiO_2 NPs, $[E_{TiO_2\ CB}]_{SHE} = -0.11$ V,[36] or photoexcited chromophores such as eosin Y, $[E_{EY^*}]_{SHE} = -1.05$ V (ref. 37) are each suitable electron donors for the various carbon supports, *i.e.* the work functions of MWNTs (Φ_{MWNT}) and SWNTs (Φ_{SWNT}) are reported in the ranges of −0.14 to 0.51 V (ref. 38) and 0.36–0.61 V (ref. 39) *vs.* SHE, respectively, while Φ_{RGO} is 0.44 V *vs.* SHE.[40] In the case of electron injection from a photoexcited semiconductor to a carbon support the charges are distributed until the two systems attain Fermi level equilibration.[14c,19a,32,33] Subsequently, these electrons may shuttle across the carbon surface, acting as an electronic conduit or "transport superhighway", and discharge at separate distinct sites on contact with suitable electron acceptors (*e.g.* various dyes molecules such as thionine, $\left[E^0_{TH/TH^{2-}}\right]_{SHE} = 0.064$ V,[41] or Ag^+ ions, $\left[E^0_{Ag^+/Ag}\right]_{SHE} = 0.80$ V)[42] or, in the absence of an electron donor, be "pooled" with the carbon support acting as an electron reservoir.

An investigation into the influence of pH on the biphasic HER in the presence of both nanowire Mo_2C and CNT/Mo_2C, as reported previously for commercial Mo_2C,[5] was attempted. The pH dependence of the redox Galvani potential difference of the hydrogen evolution reaction ($\Delta_o^w\phi_{HER}$), is predicted by the Nernst equation for the global biphasic HER (derived previously)[5] and reads

$$\Delta_o^w\phi_{HER} = \Delta_o^w\phi^0_{HER} + \frac{RT}{F}\ln\left(\frac{a^0_{DMFc^+}}{a^0_{DMFc}}\right) + \frac{RT}{F}\ln 10\text{pH} \quad (2)$$

where $\Delta_o^w\phi^0_{HER} = \left[E^0_{DMFc^+/DMFc}\right]^o_{SHE}/F$ and $a^0_{DMFc^\beta}$ represents the activity of $DMFc^+$ or DMFc (denoted by β) in 1,2-DCE. As expected, shifts in the onset potentials of the current signals of approximately 60 mV pH^{-1} were observed for both nanowire Mo_2C (Fig. 6A) and CNT/Mo_2C (Fig. 6B). However, very precise determinations of the onset potentials at each pH were somewhat hampered as with each interfacial catalyst the capacitance, primarily, and the magnitude of the PCET current wave at positive potentials, to a lesser extent, increased with time from the moment the electrochemical cell was set-up (Fig. 6C and D). The changes to the CVs were most pronounced in the first 10 min after setting up the cell when some remaining particulate catalyst in the bulk aqueous phase was brought to the interface by convective currents and trapped there (this process in the liquid–liquid electrochemical cell has been clearly captured in a movie available in the ESI†). Successive CVs varied little 30 min after setting up the cell. Thus, every effort was made to capture the CVs at approximately the same time (all CVs reported were captured less than 1 min after setting up the cell and are the 3rd scans from triplicate CV runs). Clearly, this change in

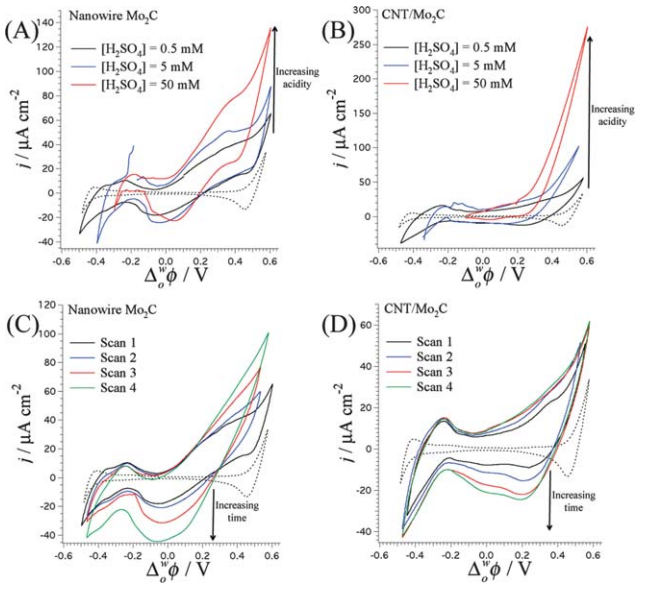

Fig. 6 Influence of pH and time on the catalytic voltammetric response. Cyclic voltammograms comparing the catalytic proton coupled electron transfer (PCET) response in the presence of either nanowire Mo_2C or CNT/Mo_2C floating at the interface ($x = 2.5$, $y = 0.1$) for (A and B) various proton concentrations in the aqueous phase ($z = 0.5$, 5, and 50) or (C and D) as a function of time ($x = 2.5$, $y = 0.1$, $z = 0.5$) with the baseline response (dashed line, $x = 0$, $y = 0$, $z = 0.5$). All electrochemical cells were setup as described in Scheme 2. Scan rate: 50 mV s^{-1}.

capacitance with time precluded performing scan rate studies for both catalysts.

Very large current densities were obtained for CNT/Mo_2C in comparison to nanowire Mo_2C for experiments carried out at *ca.* pH 1 and 2, further emphasising the exceptional activity of the carbon supported catalyst (Fig. 6A and B). In fact the evolution of H_2 for CNT/Mo_2C at *ca.* pHs 1 and 2, and also to an extent for nanowire Mo_2C at *ca.* pH 1, was so vigorous that H_2 bubbles forming *in situ* during CV scans lead to electrochemical instabilities at the liquid–liquid interface, in particular for $\Delta_o^w\phi < -0.1$ V. These electrochemical instabilities shared many common features with those occurring for the transfer of surface active ions (*e.g.* alkylammonium or alkylsulphate ions)[43] at a polarised liquid–liquid interface, as documented by Kakiuchi's group.[44] They manifest themselves as irregular increases in current that, strikingly, are restricted to a certain limited potential region and are caused by the hydrodynamic movement of the liquid phase adjacent to the interface. A spontaneous interfacial convective movement arises due to the Marangoni effect (*i.e.* an interfacial surface tension (γ) gradient along an interface between two fluids that produces an interfacial flow in the direction of the gradient from lower to higher γ)[45] and propagates into the bulk due to viscous forces. This phenomenon is clearly observed in Fig. 7 where the electrochemical instabilities initially begin approaching the standard ion transfer potential of $DMFc^+$ ($\Delta_o^w\phi^{0'}_{tr,DMFc^+} = -0.26$ V) (ref. 6) on the negative-going sweep but disappear in the positive potential region of the scan. For surface active ions, the unstable section of the potential window occurs in the potential region where the ionic surfactants adsorb at the interface and cause a decrease in γ. It is worth noting, however, that the instability of the interface is not caused by an ultralow γ but, as Kakiuchi states, "*more precisely, for stability, the system needs to satisfy the upward convexity of the electrocapillary curve, because γ is the excess surface Gibbs energy that determines the stability of the interface.*"[44] Thus, we tentatively assume that the upward convexity of the electrocapillary curve is no longer maintained during the flux of $DMFc^+$ across the interface in the presence of interfacially adsorbed bubbles. The precise reason is as yet unclear and will be the subject of a future study using quasi-elastic light scattering (QELS) to measure electrocapillary curves with this system. Finally, at *ca.* pH 1, with CNT/Mo_2C floating at the interface, the CV potentials were reversed at $\Delta_o^w\phi \approx -0.1$ V to obtain clear CVs of the catalytic PCET process (Fig. 7).

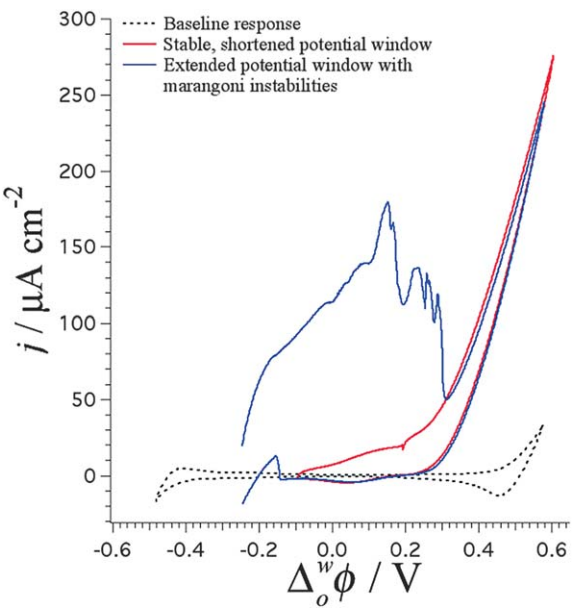

Fig. 7 Cyclic voltammograms highlighting the electrochemical instability of the liquid–liquid interface due to Marangoni-type movements of the interface when the potential is scanned to values of $\Delta_o^w\phi < -0.1$ V in the presence of a high proton concentration, the electron donor DMFc and a powerful H_2 evolution catalyst, such as CNT/Mo_2C in this case ($x = 2.5$, $y = 0.1$, $z = 50$). All electrochemical cells were set up as described in Scheme 2. Scan rate: 50 mV s^{-1}.

The movement of CNT microparticles upon polarisation of the liquid–liquid interface

The influence of polarising the liquid–liquid interface on the movement of the adsorbed catalytic rafts was visualised by monitoring the movement of CNTs adsorbed at the interface for an electrochemical cell (see Scheme 2, $x = 2.5$, $y = 0.1$, and $z = 0.5$), in this case, under aerobic conditions. The movement of the CNTs was followed in real time as the applied potential difference across the interface ($\Delta_o^w\phi$) was swept repeatedly for consecutive CV scans, as shown in a movie available in the ESI.† The positions of the CNTs at the interface for specific applied potential differences are shown in Fig. 8. The first observation was that the interface was not polarised uniformly across its surface. This was due to the design of the glass electrochemical cell (see Fig. 8 and S2, ESI,† for close-up images of the interface in the cell clearly showing the relative positions of the Pt electrodes and Luggin capillaries). The Pt counter electrodes in each phase were positioned to the left of centre over the circular interface on the opposite side to the Luggin capillaries. As a result, the applied interfacial potential difference was inhomogeneously distributed across the interface, being most strongly felt directly beneath the Pt wires and its influence diminished with distance from that point on the interface. In

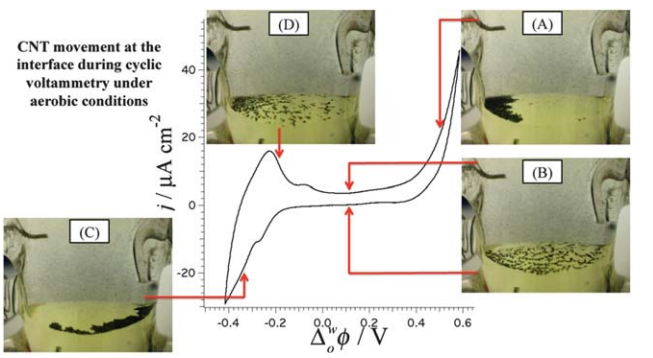

Fig. 8 Images of the movement and specific positioning of CNTs at the liquid–liquid interface for various potential regimes, *i.e.* (A) $\Delta_o^w\phi \gg 0.3$ V, (B) -0.1 V $\leq \Delta_o^w\phi \leq -0.3$ V, (C) $\Delta_o^w\phi \ll -0.1$ V and (D) at $\Delta_o^w\phi^{0'}_{tr,DMFc^+} = -0.26$ V, during a cyclic voltammogram (scan rate: 50 mV s^{-1}). A movie capturing the movement of the CNTs at the liquid–liquid interface is available in the ESI.†

the region of the CV where no Faradaic processes were taking place, *i.e.* the point of zero charge (pzc) in Fig. 8B, no movement of the CNTs was evident and they were uniformly dispersed across the interface. On polarising the interface positively (*i.e.* the aqueous phase was polarised positively relative to the organic phase), an interfacial movement of the negative charged CNTs in the direction of the Pt electrodes occurred, suggesting an electrostatic attraction as the dominant force influencing the movement of the CNTs (Fig. 8A). Conversely, on polarising the interface negatively, an interfacial movement of the CNTs occurred in the opposite direction, away from the Pt electrodes (Fig. 8C). Finally, at $\Delta_o^w\phi^{0'}_{tr,DMFc^+} = -0.26$ V on the positive going CV sweep, the flux of $DMFc^+$ across the interface caused a temporary interfacial movement of the CNTs once more in the direction of the Pt electrodes (Fig. 8D).

Biphasic mechanism of proton reduction for a floating CNT/Mo_2C catalytic raft

A reaction scheme outlining the biphasic reduction of protons incorporating a CNT/Mo_2C conductive catalytic nano-raft floating at the polarised liquid–liquid interface is illustrated in Scheme 3. The work functions of Mo_2C and the CNT support are similar; Φ_{Mo_2C} has been reported as 0.27 (±0.02) V *vs.* SHE,[46] while Φ_{MWNT} is reported in the range of −0.14 to 0.51 V *vs.* SHE,[38] as noted. Thus, depending on the precise value of Φ_{SWNT}, the excess negative charge will flow from the CNT support to Mo_2C or *vice versa* until the Fermi levels have equalized and a nano-Schottky junction with the appropriate band bending has formed. The redox potential of organic solubilized DMFc is sufficiently negative to reduce the CNTs utilised in this study (as proven, *vide supra*, by 4-electrode voltammetry experiments). Thus, the electron ultimately consumed in the PCET process may (a) be provided by DMFc directly to an adsorbed hydrogen atom at the Mo_2C catalytically active site (H*) or (b) be injected from DMFc to a state in the CNTs close to the Fermi level and, crucially, non-specifically at any site on the carbon surface. The latter electrons are "pooled" in the CNT and, being highly mobile along the CNT "electron superhighway", will subsequently transfer to an empty state in Mo_2C. Finally, electron transfer occurs to H*. In the absence of a carbon support, *i.e.* for commercial Mo_2C and nanowire Mo_2C, the only route available for electron injection is by the direct interaction of DMFc with H*. The precise mechanism of hydrogen evolution on the surface of Mo_2C has yet to be elucidated with several unanswered questions remaining. Are bridging hydride species such as Mo–H–C involved?[27] How exactly is molecular H_2 released; does a $2H^* \rightarrow H_2 + 2^*$ or $H^+ + e^- + H^* \rightarrow H_2 + *$ process dominate (as similarly investigated for MoS_2 by density functional theory (DFT) calculations)?[47] As noted above, energetically only organic solubilised protons or protons under the influence of an applied $\Delta_o^w\phi > 0.55$ V may be reduced.

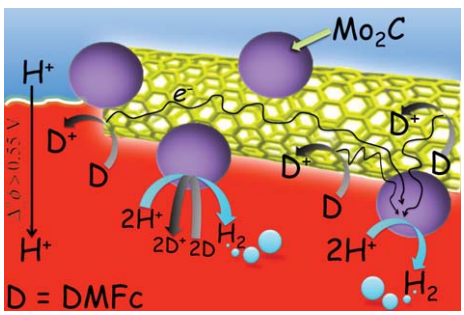

Scheme 3 Schematic of the biphasic H_2 evolution reaction in the presence of the conductive catalytic CNT/Mo_2C nanocomposite floating at a polarised interface. The electron donor, DMFc, may inject electrons anywhere on the carbon support and these electrons are then efficiently shuttled along the conductive CNT electron "transport superhighway" to the Mo_2C active sites where proton coupled electron transfer (PCET) H_2 evolution occurs. Alternatively, DMFc may take part directly in a PCET process at the Mo_2C active site to evolve H_2. The aqueous and organic phases are coloured blue and red, respectively.

Conclusions

Gas chromatography, UV/vis kinetic and cyclic voltammetry studies all successfully demonstrate that CNT/Mo_2C is a superior biphasic HEC to nanowire Mo_2C, and, as expected, vastly superior to commercial Mo_2C. Since both CNT/Mo_2C and nanowire Mo_2C possess nano-Mo_2C sites, the primary difference between these two catalysts is the presence of the carbon support in CNT/Mo_2C. Thus, we may logically speculate that the provision of electrons *via* the CNT "electron superhighway" is a much more efficient process than DMFc directly interacting with the catalytically active site. In essence the ability of DMFc to react non-specifically with any site on the CNT/Mo_2C support dramatically increases the effective cross-section of the reaction between the electron donor and supported nano-catalyst, and thus the rate of reaction, in comparison to the "free" nano-catalyst.

This study clearly highlights that, once electrons are provided to the carbon support of a floating conductive catalytic raft, biphasic H_2 evolution proceeds immediately and with an effortless efficiency. Thus, perspectives for this work will focus on alternative methods of providing electrons to the carbon support using weaker electron donors than DMFc in the presence of light-activated multifunctional semiconductor/catalyst/carbon or dye/catalyst/carbon nanocomposites. Such biphasic systems are particularly exciting, not solely for H_2 evolution but also for other light-activated catalytic processes (*e.g.* the oxygen evolution reaction (OER)[48] or CO_2 reduction[49]), as they facilitate the efficient separation of charges, the step that mainly determines the quantum yield in photochemical reactions, two-fold; (a) by providing a platform that theoretically allows the photoproducts of the reaction to be separated in different phases, as in the light-harvesting complex of photosynthetic organisms,[50] and (b) the carbon substrate creates a directionality of the electron transfer, *i.e.* recombination reactions in a light-activated semiconductor can be minimized for example. Finally, the production of H_2 using weak electron donors is beneficial as relatively weak electron acceptors (generated from a second half-reaction, for example the light driven OER) would be required to regenerate both donor and acceptor species, thereby "re-setting" the photo-system.

Acknowledgements

This work was supported by the NSFC 20925517, 973 programme (2013CB934101), SKLEAC201101, and the Swiss National Science Foundation (SNF) grant "Solar Fuels" 200 021-134 745.

Notes and references

1 (*a*) J. A. Turner, *Science*, 2004, **305**, 972–974; (*b*) N. S. Lewis and D. G. Nocera, *Proc. Natl. Acad. Sci. U. S. A.*, 2006, **103**, 15729–15735; (*c*) G. W. Crabtree and M. S. Dresselhaus, *MRS Bull.*, 2011, **33**, 421–428; (*d*) A. Sartbaeva, V. L. Kuznetsov, S. A. Wells and P. P. Edwards, *Energy Environ. Sci.*, 2008, **1**, 79–85; (*e*) M. Pagliaro, A. G. Konstandopoulos, R. Ciriminna and G. Palmisano, *Energy Environ. Sci.*, 2010, **3**, 279–287.

2 (*a*) B. Su, R. Partovi-Nia, F. Li, M. Hojeij, M. Prudent, C. Corminboeuf, Z. Samec and H. H. Girault, *Angew. Chem.*, 2008, **120**, 4753–4756; (*b*) I. Hatay, B. Su, F. Li, R. Partovi-Nia, H. Vrubel, X. Hu, M. Ersoz and H. H. Girault, *Angew. Chem., Int. Ed.*, 2009, **48**, 5139–5142; (*c*) M. A. Méndez, R. Partovi-Nia, I. Hatay, B. Su, P. Ge, A. Olaya, N. Younan, M. Hojeij and H. H. Girault, *Phys. Chem. Chem. Phys.*, 2010, **12**, 15163–15171; (*d*) B. Su, I. Hatay, P. Y. Ge, M. Méndez, C. Corminboeuf, Z. Samec, M. Ersoz and H. H. Girault, *Chem. Commun.*, 2010, **46**, 2918–2919.

3 P. Ge, T. K. Todorova, I. H. Patir, A. J. Olaya, H. Vrubel, M. Mendez, X. Hu, C. Corminboeuf and H. H. Girault, *Proc. Natl. Acad. Sci. U. S. A.*, 2012, **109**, 11558–11563.

4 I. Hatay, P. Y. Ge, H. Vrubel, X. Hu and H. H. Girault, *Energy Environ. Sci.*, 2011, **4**, 4246–4251.

5 M. D. Scanlon, X. Bian, H. Vrubel, V. Amstutz, K. Schenk, X. Hu, B. Liu and H. H. Girault, *Phys. Chem. Chem. Phys.*, 2013, **15**, 2847–2857.

6 P. Ge, M. D. Scanlon, P. Peljo, X. Bian, H. Vubrel, A. O'Neill, J. N. Coleman, M. Cantoni, X. Hu, K. Kontturi, B. Liu and H. H. Girault, *Chem. Commun.*, 2012, **48**, 6484–6486.

7 S. Min and G. Lu, *J. Phys. Chem. C*, 2012, **116**, 25415–25424.

8 V. Georgakilas, D. Gournis, V. Tzitzios, L. Pasquato, D. M. Guldi and M. Prato, *J. Mater. Chem.*, 2007, **17**, 2679–2694.

9 I. V. Lightcap and P. V. Kamat, *Acc. Chem. Res.*, 2012, DOI: 10.1021/ar300248f.

10 P. V. Kamat, I. Bedja and S. Hotchandani, *J. Phys. Chem.*, 1994, **98**, 9137–9142.

11 S. N. Baker and G. A. Baker, *Angew. Chem., Int. Ed.*, 2010, **49**, 6726–6744.

12 X. Bian, J. Zhu, L. Liao, M. D. Scanlon, P. Ge, C. Ji, H. H. Girault and B. Liu, *Electrochem. Commun.*, 2012, **22**, 128–132.

13 (*a*) L. Liao, J. Zhu, X. Bian, L. Zhu, M. D. Scanlon, H. H. Girault and B. Liu, *Adv. Funct. Mater.*, 2013, DOI: 10.1002/adfm.201300318; (*b*) Z. Chen, W. Ren, L. Gao, B. Liu, S. Pei and H.-M. Cheng, *Nat. Mater.*, 2011, **10**, 424–428.

14 (*a*) H. Hayashi, I. V. Lightcap, M. Tsujimoto, M. Takano, T. Umeyama, P. V. Kamat and H. Imahori, *J. Am. Chem. Soc.*, 2011, **133**, 7684–7687; (*b*) A. Iwase, Y. H. Ng, Y. Ishiguro, A. Kudo and R. Amal, *J. Am. Chem. Soc.*, 2011, **133**, 11054–11057; (*c*) I. V. Lightcap, T. H. Kosel and P. V. Kamat, *Nano Lett.*, 2010, **10**, 577–583.

15 G. Che, B. B. Lakshmi, C. R. Martin and E. R. Fisher, *Langmuir*, 1999, **15**, 750–758.

16 (*a*) M. Quintana, X. Ke, G. Van Tendeloo, M. Meneghetti, C. Bittencourt and M. Prato, *ACS Nano*, 2010, **4**, 6105–6113; (*b*) R. Muszynski, B. Seger and P. V. Kamat, *J. Phys. Chem. C*, 2008, **112**, 5263–5266.

17 G. M. Scheuermann, L. Rumi, P. Steurer, W. Bannwarth and R. Mülhaupt, *J. Am. Chem. Soc.*, 2009, **131**, 8262–8270.

18 Y. Li, H. Wang, L. Xie, Y. Liang, G. Hong and H. Dai, *J. Am. Chem. Soc.*, 2011, **133**, 7296–7299.

19 (*a*) A. Kongkanand and P. V. Kamat, *ACS Nano*, 2007, **1**, 13–21; (*b*) G. Williams, B. Seger and P. V. Kamat, *ACS Nano*, 2008, **2**, 1487–1491.

20 P. V. Kamat, *J. Phys. Chem. Lett.*, 2011, **2**, 242–251.

21 (*a*) A. Mukherji, B. Seger, G. Q. Lu and L. Wang, *ACS Nano*, 2011, **5**, 3483–3492; (*b*) Q. Xiang, J. Yu and M. Jaroniec, *J. Am. Chem. Soc.*, 2012, **134**, 6575–6578; (*c*) Q. Xiang and J. Yu, *J. Phys. Chem. Lett.*, 2013, **4**, 753–759.

22 I. V. Lightcap, S. Murphy, T. Schumer and P. V. Kamat, *J. Phys. Chem. Lett.*, 2012, **3**, 1453–1458.

23 (*a*) Y. Lin, H. Skaff, T. Emrick, A. D. Dinsmore and T. P. Russell, *Science*, 2003, **299**, 226–229; (*b*) H. Duan, D. Wang, D. G. Kurth and H. Möhwald, *Angew. Chem., Int. Ed.*, 2004, **43**, 5639–5642; (*c*) W. H. Binder, *Angew. Chem., Int. Ed.*, 2005, **44**, 5172–5175; (*d*) D. Wang, H. Duan and H. Mohwald, *Soft Matter*, 2005, **1**, 412–416; (*e*) S. Biswas and L. T. Drzal, *Nano Lett.*, 2009, **9**, 167–172; (*f*) M. M. Gudarzi and F. Sharif, *Soft Matter*, 2011, **7**, 3432–3440.

24 Y. K. Kim and H. Park, *Appl. Catal., B*, 2012, **125**, 530–537.

25 Q. Gao, C. Zhang, S. Xie, W. Hua, Y. Zhang, N. Ren, H. Xu and Y. Tang, *Chem. Mater.*, 2009, **21**, 5560–5562.

26 Q. Gao, C. Zhang, S. Wang, W. Shen, Y. Zhang, H. Xu and Y. Tang, *Chem. Commun.*, 2010, **46**, 6494–6496.

27 H. Vrubel and X. Hu, *Angew. Chem., Int. Ed.*, 2012, **51**, 12703–12706.

28 J. J. Nieminen, I. Hatay, P. Ge, M. A. Méndez, L. Murtomaki and H. H. Girault, *Chem. Commun.*, 2011, **47**, 5548–5550.

29 (*a*) K. H. An, W. S. Kim, Y. S. Park, J. M. Moon, D. J. Bae, S. C. Lim, Y. S. Lee and Y. H. Lee, *Adv. Funct. Mater.*, 2001, **11**, 387–392; (*b*) E. Frackowiak and F. Béguin, *Carbon*, 2002, **40**, 1775–1787; (*c*) D. N. Futaba, K. Hata, T. Yamada, T. Hiraoka, Y. Hayamizu, Y. Kakudate, O. Tanaike, H. Hatori, M. Yumura and S. Iijima, *Nat. Mater.*, 2006, **5**, 987–994.

30 W. F. Chen, C. H. Wang, K. Sasaki, N. Marinkovic, W. Xu, J. T. Muckerman, Y. Zhu and R. R. Adzic, *Energy Environ. Sci.*, 2013, **6**, 943–951.

31 (*a*) D. Dubois, K. M. Kadish, S. Flanagan and L. J. Wilson, *J. Am. Chem. Soc.*, 1991, **113**, 7773–7774; (*b*) Q. Xie, E. Perez-Cordero and L. Echegoyen, *J. Am. Chem. Soc.*, 1992, **114**, 3978–3980.

32 S. Krishnamurthy, I. V. Lightcap and P. V. Kamat, *J. Photochem. Photobiol., A*, 2011, **221**, 214–219.
33 A. Kongkanand and P. V. Kamat, *J. Phys. Chem. C*, 2007, **111**, 9012–9015.
34 S. Trasatti, *Pure Appl. Chem.*, 1986, **58**, 955–966.
35 P. Wardman, *J. Phys. Chem. Ref. Data*, 1989, **18**, 1637–1756.
36 Y. Shimizu, T. Hyodo and M. Egashira, *Sens. Actuators, B*, 2007, **121**, 219–230.
37 G. D. Sharma, P. Balraju, M. Kumar and M. S. Roy, *Mater. Sci. Eng., B*, 2009, **162**, 32–39.
38 (*a*) P. Chen, X. Wu, X. Sun, J. Lin, W. Ji and K. L. Tan, *Phys. Rev. Lett.*, 1999, **82**, 2548–2551; (*b*) R. Gao, Z. Pan and Z. L. Wang, *Appl. Phys. Lett.*, 2001, **78**, 1757–1759; (*c*) S. Suzuki, Y. Watanabe, T. Kiyokura, K. G. Nath, T. Ogino, S. Heun, W. Zhu, C. Bower and O. Zhou, *Phys. Rev. B: Condens. Matter*, 2001, **63**, 245418; (*d*) Z. Xu, X. D. Bai, E. G. Wang and Z. L. Wang, *Appl. Phys. Lett.*, 2005, **87**, 163106–163103.
39 (*a*) S. Suzuki, C. Bower, Y. Watanabe and O. Zhou, *Appl. Phys. Lett.*, 2000, **76**, 4007–4009; (*b*) M. Shiraishi and M. Ata, *Carbon*, 2001, **39**, 1913–1917; (*c*) J. Zhao, J. Han and J. P. Lu, *Phys. Rev. B: Condens. Matter*, 2002, **65**, 193401.
40 B.-S. Kong, J. Geng and H.-T. Jung, *Chem. Commun.*, 2009, 2174–2176.
41 P. V. Kamat, *J. Chem. Soc., Faraday Trans. 1*, 1985, **81**, 509–518.
42 P. W. Atkins, *Physical Chemistry*, Oxford University Press, Oxford, 1990.
43 Y. Kitazumi and T. Kakiuchi, *Langmuir*, 2009, **25**, 8062–8068.
44 Y. Kitazumi and T. Kakiuchi, *Bull. Chem. Soc. Jpn.*, 2011, **84**, 1312–1320.
45 L. E. Scriven and C. V. Sternling, *Nature*, 1960, **187**, 186–188.
46 (*a*) D. W. Vance, *Phys. Rev.*, 1967, **164**, 372–380; (*b*) R. G. Wilson and W. E. McKee, *J. Appl. Phys.*, 1967, **38**, 1716–1718; (*c*) R. G. Wilson, *J. Appl. Phys.*, 1968, **39**, 2306–2310; (*d*) H. Kawano, *Prog. Surf. Sci.*, 2008, **83**, 1–165.
47 B. Hinnemann, P. G. Moses, J. Bonde, K. P. Jørgensen, J. H. Nielsen, S. Horch, I. Chorkendorff and J. K. Nørskov, *J. Am. Chem. Soc.*, 2005, **127**, 5308–5309.
48 Y. Liang, Y. Li, H. Wang, J. Zhou, J. Wang, T. Regier and H. Dai, *Nat. Mater.*, 2011, **10**, 780–786.
49 X.-J. Lv, W.-F. Fu, C.-Y. Hu, Y. Chen and W.-B. Zhou, *RSC Adv.*, 2013, **3**, 1753–1757.
50 (*a*) D. Fraçkowiak and E. Rabinowitch, *J. Phys. Chem.*, 1966, **70**, 3012–3014; (*b*) A. G. Volkov, M. I. Gugeshashvili and D. W. Deamer, *Electrochim. Acta*, 1995, **40**, 2849–2868.